AGU100 ADVANCING EARTH AND SPACE SCIENCE

Geophysical Research Letters

RESEARCH LETTER
10.1029/2018GL077276

Key Points:
- Impingement of a mantle plume under a lithosphere subjected to tension focuses brittle strain in the crust
- Rift width variation results from spatial variations of the lithospheric geotherm associated with the evolving mantle plume
- Modeled strain localization is consistent with the observed transition from the narrow Kenya rift to broader rifts to the north and south

Correspondence to:
A. Koptev,
alexander.koptev@ifg.uni-tuebingen.de

Citation:
Koptev, A., Calais, E., Burov, E., Leroy, S., & Gerya, T. (2018). Along-axis variations of rift width in a coupled lithosphere-mantle system, application to East Africa. *Geophysical Research Letters*, *45*, 5362–5370. https://doi.org/10.1029/2018GL077276

Received 24 JAN 2018
Accepted 23 MAY 2018
Accepted article online 29 MAY 2018
Published online 5 JUN 2018

Along-Axis Variations of Rift Width in a Coupled Lithosphere-Mantle System, Application to East Africa

Alexander Koptev[1,2], Eric Calais[3], Evgueni Burov[1,4], Sylvie Leroy[1], and Taras Gerya[5]

[1]CNRS, Institut des Sciences de la Terre de Paris (ISTeP), Sorbonne Université, Paris, France, [2]Department of Geosciences, University of Tübingen, Tübingen, Germany, [3]Ecole normale supérieure, Department of Geosciences, CNRS UMR8538, Université PSL, Paris, France, [4]Deceased 9 October 2015, [5]Institute of Geophysics, ETH-Zurich, Zurich, Switzerland

Abstract Narrow and wide rifts are end-member expressions of continental extension. Within the framework of passive rifting, the transition from wide to narrow rifts requires lowering the geothermal gradient. Reconciling this view with observational evidence for narrow rift zones in regions underlain by sublithospheric hot plume material, such as the eastern branch of the East African Rift, requires invoking preexisting weak zones for strain to localize in a warm crust. Based on thermomechanical numerical models, we show that along-rift width variations can develop spontaneously as a consequence of spatial variations of the geotherm over an evolving mantle plume impinging a lithosphere subjected to ultraslow extension. The eastern branch of the East African Rift, with a narrow Kenya segment underlain by a mantle plume head and widening to the north and south in the colder regions of the Turkana depression and North Tanzania divergence, is in agreement with this numerical prediction.

Plain Language Summary This study is inspired by a contradiction between the usual inference from passive rifting models that predict a transition from narrow to wide rifts correlated with increasing lithospheric temperatures, while observations in the eastern branch of the East African Rift show that its narrowest segment is underlain by a deep-seated positive thermal anomaly. We present the results from 3-D thermomechanical numerical experiments showing that narrow rifting, conventionally attributed to "passive" rifting of cold and strong lithosphere, can also develop in hot and weak lithosphere in the case of plume-assisted rifting, as observed in the Kenyan rift. Preexisting lithospheric structures are not required to determine and control rift initiation and development, in contrast to the classical interpretation based on passive models that require preexisting rheologically weak zones to initiate and guide fault propagation.

1. Introduction

Variations in the width of continental rifts from narrow (e.g., Main Ethiopian Rift) to wide (e.g., Basin and Range) are classically explained in terms of the temperature and strength of the lithosphere undergoing tensional stress (Buck, 1991). Some numerical experiments (Gueydan et al., 2008) indeed show that a hot and weak lithosphere (i.e., Moho temperature $>$ 700°C) promotes distributed deformation and a broad rift zone in the upper crust while narrow rifts occur under low (i.e., $<$700°C) Moho temperature. However, recent high-resolution, 3-D experiments of lithospheric stretching with free surface and a thermomechanically coupled mantle-lithosphere show that narrow rifts, conventionally associated with cold and strong lithosphere, can develop as a result of plume impingement, which acts to weaken the lithosphere and focus brittle strain in the crust (Burov & Gerya, 2014).

Here we test this mixed mechanism of active-passive rifting using observations from the eastern branch of the East African Rift System (EARS, Figure 1) as guidelines for model setup and validation. The EARS, the ~3,000-km-long active volcano-tectonic structure that marks the extensional boundary between the Nubian and Somalian plates (Braile et al., 2006; Dawson, 1992; Ring, 2014), cuts across the high elevation (~1,500 m) East African plateaus, a long wavelength topography dynamically supported by a broad low-velocity seismic anomaly imaged in the lower mantle, the African Superplume (Lithgow-Bertelloni & Silver, 1998; Ritsema et al., 1999; Van der Hilst et al., 1997). A robust feature of its upper mantle, despite some differences in body-wave and surface-wave tomographic models (e.g., Kendall et al., 2006), is the presence of the low-velocity Kenyan plume under the central part of the EARS (e.g., Chang et al., 2015; Nyblade et al., 2000;

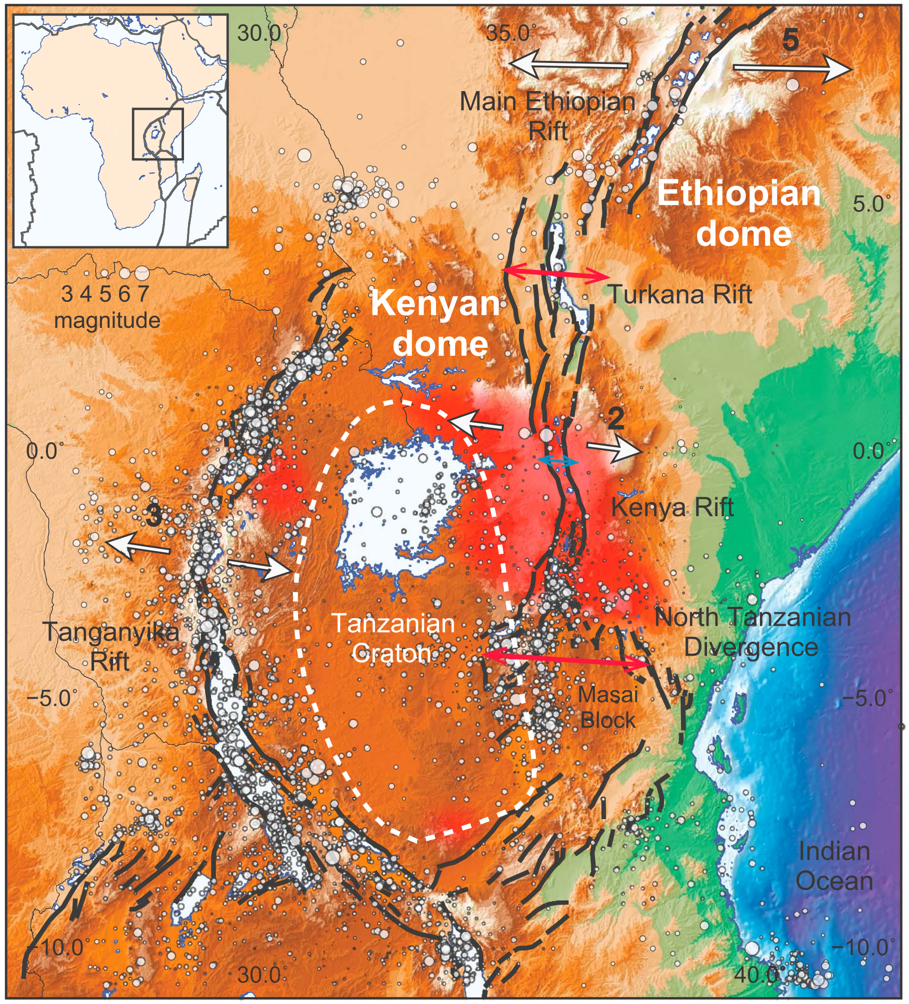

Figure 1. Tectonic setting of the East African Rift System. The black lines indicate major faults (Corti et al., 2007). The white dashed line shows the edges of the Tanzanian craton. Low-velocity zones (less than 4.4 km/s at a depth of 200 km) in red were imaged by *S* wave tomography analysis from O'Donnell et al. (2013). The white circles show earthquake epicenters. The top left inset illustrates the location of the studied area within Africa. The red arrows indicate wide rifting in the Turkana depression and the North Tanzania divergence zone, whereas the blue arrow indicates narrow rifting in the Kenya segment.

O'Donnell et al., 2013; Ritsema et al., 1998), possibly rooted in the deeper African Superplume according to He, Ar, and Ne isotopic data from Neogene volcanics (Halldórsson et al., 2014).

Rifting in the western branch localizes within preexisting Proterozoic mobile belts sutures and shear zones at the margin of the Tanzanian craton (e.g., Katumwehe et al., 2015; Morley,2010), leading to narrow elongated basins such as the *Tanganyika* and its southern prolongation in the Malawi *rift* (Laó-Dávila et al., 2015; Ring et al., 1992; Versfelt & Rosendahl, 1989). On the contrary, the eastern branch shows the along-axis transition from a wide rift (200–350 km) in the Turkana depression between the Kenyan and Ethiopian domes (Hendrie et al., 1994; Morley et al., 1992), to a narrow rift (60–70 km) at the Tanzanian craton margin in the Kenya rift (Melnick et al., 2012; Zeyen et al., 1997), then further south to the 300 to 400-km-wide Tanzania divergence zone (Corti et al., 2013; Dawson, 1992; Isola et al., 2014; Le Gall et al., 2004, 2008). Within this wide-narrow-wide rift system, the narrow Kenya rift cuts across a topographic dome interpreted as the signature of the underlying Kenyan plume head according to geochemical (e.g., George et al., 1998; MacDonald et al., 2001; Pik et al., 2006) and geophysical data (e.g., Chang & Van der Lee, 2011; Nyblade et al., 2000).

The explanation for this wide-narrow-wide transition has often been that modern rift basins remobilize pre-existing crustal structures inherited from a poly-phased geological history (e.g., Ebinger et al., 2000; Morley et al., 1992). For instance, the fact that the present-day Turkana rift is superimposed on a complex

10.1029/2018GL077276

Table 1
Rheological and Material Properties Used in the Models

			Rheological parameters											Thermal parameters		
				Ductile				Brittle								
								C (MPa)		Sin(φ)		ε				
Material		ρ_0 (kg/m^3)	Flow law	E (kJ/mol)	n	A_D (Pa^n × s)	V (J/(MPa x mol))	C_0	C_1	b_0	b_1	ε_0	ε_1	k (W/(m × K))	H_r (μW/m^3)	H_L (kJ/kg)
Upper crust		2,750	Wet quartzite (WetQz)	154	2.3	1.97×10^{17}	0	10	3	0.6	0.3	0.0	0.25	0.64 + 807/(T + 77)	2.00	300
Lower crust	1	2,950	Wet quartzite (WetQz)	154	2.3	1.97×10^{17}	0	10	3	0.6	0.3	0.0	0.25	—//—	1.00	300
	2	3,000	Plagioclase (An_{75})	238	3.2	4.80×10^{22}	0	10	3	0.6	0.3	0.0	0.25	1.18 + 474/(T + 77)	0.25	380
Lithosphere-sublithosphere mantle		3,300	Dry olivine	532	3.5	3.98×10^{16}	1.6	10	3	0.6	0.3	0.0	0.25	0.73 + 1293/(T + 77)	0.022	380
Plume mantle		3,200	Wet olivine	470	4.0	5.01×10^{20}	1.6	3	3	0.1	0.0	0.0	0.25	—//—	0.024	300

Note. ρ_0 is reference density (at P_0 = 0.1 MPa and T_0 = 298 K), E is activation energy, n is power law exponent, A_D is material constant, V is activation volume, C is cohesion, φ is friction angle, ε is strain, C_0, C_1 are maximal and minimal cohesion (linear softening law), b_0, b_1 are maximal and minimal sines of frictional angle (linear softening law), ε_0, ε_1 are minimal and maximal strains (linear softening law), k is thermal conductivity, H_r is radiogenic heat production, and H_L is the latent heat of melting of rock.

Mesozoic rift system associated with Gondwana rupture that extended from Sudan through Turkana and eastern Kenya led to the proposal that its breadth was a result of the superposition of ancient and modern structures (e.g., Ebinger et al., 2000; Hendrie et al., 1994). However, the modern Turkana rift is oblique to these Mesozoic extensional structures. Modern extension started in Turkana in the upper Eocene (Furman et al., 2006) within a “broadly rifted zone” (Rooney, 2017) marked by widespread volcanism that included southernmost Ethiopia (Morley et al., 1999). Rift basins started forming in the late Oligocene, crosscutting the Mesozoic Anza rift (Morley et al., 1992; Vetel et al., 2004). Faulting and seismicity currently concern a 200 to 350-km-wide zone (Figure 1).

Analog and numerical models of rifting in the EARS have focused on the lithosphere, imposing inherited lateral strength variations (e.g., Brune et al., 2017), and neglecting the active role of the mantle, at odds with the unequivocal presence of deep-seated low-velocity anomalies underneath the rift (e.g., Nyblade et al., 2000; O’Donnell et al., 2013; Ritsema et al., 1999). Here we ask whether along-axis rift variations in Cenozoic rifts are necessarily determined by crustal structures inherited from past tectonic events or if that spatial variability can develop spontaneously as a result of the interaction of an active mantle plume with a continental lithosphere that is initially laterally homogeneous. To address this question we use high-resolution, 3-D thermomechanical numerical models of active-passive rifting with a setup inspired from large-scale EARS structures. We intentionally keep the model geometry as simple as possible and avoid prescribing preexisting zones of crustal weakness.

2. Methods

We implement high-resolution, rheologically stratified, 3-D thermomechanical numerical models using the staggered grid/particle-in-cell viscous-plastic 3DELVIS code (Gerya, 2010; Gerya & Yuen, 2007), based on a combination of a finite difference method with a marker-in-cell technique. We chose rheological parameters (Table 1) in consideration of previous successful experiments of plume-lithosphere interaction (e.g., Beniest, Koptev, & Burov, 2017; Beniest, Koptev, Leroy, et al., 2017; Burov, 2011; Burov & Cloetingh, 2010; Burov & Gerya, 2014; Burov & Guillou-Frottier, 2005; François et al., 2017; Koptev, Burov, et al., 2017; Koptev, Cloetingh, et al., 2017). The initial model setup and geotherm are consistent with observation-based estimates of the regional thermal and rheological structures of the crust and the lithosphere (Albaric et al., 2009; Artemieva, 2006; Fishwick & Bastow, 2011; Pérez-Gussinyé et al., 2009) and with surface heat flow (Nyblade, 1997) in East Africa.

The model domain is 1,500 × 1,500 km wide by 635 km deep with a 3 × 3 × 3 km grid resolution. It contains a 150-km-thick lithosphere with a two-layer, 36-km-thick crust. We initiate a plume by seeding a 200-km-radius

Table 2
Main Controlling Parameters of the Experiments

Model number	Model series	Model title	Controlling parameters: Presence of the Tanzanian craton	Temperature at the Moho (°C)	Horizontal extension velocity (mm/yr)
1	Generic	Gen.T_{Mh} = 600°C, V_{ext} = 1.5 mm/yr	No	600	1.5
2	Generic	Gen.T_{Mh} = 700°C, V_{ext} = 1.5 mm/yr	No	700	1.5
3	Generic	Gen.T_{Mh} = 800°C, V_{ext} = 1.5 mm/yr	No	800	1.5
4	Generic	Gen.T_{Mh} = 600°C, V_{ext} = 3 mm/yr	No	600	3
5	Generic	Gen.T_{Mh} = 700°C, V_{ext} = 3 mm/yr	No	700	3
6	Generic	Gen.T_{Mh} = 800°C, V_{ext} = 3 mm/yr	No	800	3
7	Generic	Gen.T_{Mh} = 600°C, V_{ext} = 6 mm/yr	No	600	6
8	Generic	Gen.T_{Mh} = 700°C, V_{ext} = 6 mm/yr	No	700	6
9	Generic	Gen.T_{Mh} = 800°C, V_{ext} = 6 mm/yr	No	800	6
10	EARS-oriented	EARS.T_{Mh} = 700°C, V_{ext} = 3 mm/yr	Yes	700	3

temperature anomaly at the base of the upper mantle, 300 K warmer than the surroundings. We simulate tectonic forcing by applying constant divergent velocity normal to two opposing model boundaries at a rate derived from Neogene plate kinematic reconstructions (DeMets & Merkouriev, 2016; Saria et al., 2014).

We perform two sets of 3-D numerical experiments (Table 2). First, we run generic models with an initial laterally homogeneous lithosphere (models 1–9). As Moho temperature is assumed to be a key parameter controlling surface strain and the associated fault pattern (e.g., Buck, 2006; Gueydan et al., 2008), we use these models to investigate the influence of the thermal structure of the continental lithosphere on the style of plume-induced deformation in the upper crust. Second, we run one slightly more complex experiment (model 10) that includes an oval-shape, 250-km-thick craton with a lateral extent of 800 × 400 km that mimics the Tanzanian craton and a mantle plume initially laterally shifted to the northeast with respect to the center of the model box (Adams et al., 2012; Artemieva, 2006; Mulibo & Nyblade, 2013; Ritsema et al., 1998). This model, similar in setup to those of Koptev et al. (2015, 2016), is meant to simulate a setting close to that of the eastern branch of the EARS.

Except for the simulated mantle plume and the craton, the models do not contain initial lateral variations in mechanical properties or preexisting zones of weakness. Because we consider a relatively short time interval (5 Myr), the relative motion of the African continent with respect to the plume source is small over the course of our model evolution, on the order of 100 km given the ~2-cm/yr absolute velocity of the African plate over the past 20 Myr (O'Connor et al., 1999). We therefore assume a stationary plume-lithosphere system in the simulations. The size and temperature of the mantle plume have been chosen in order to agree with observed data for both the final distribution of hot material ponding at the lithosphere-asthenosphere boundary (e.g., O'Donnell et al., 2013) and the observed temperature anomaly at the 410-km discontinuity (Huerta et al., 2009).

3. Results

We tested nine generic setups (models 1–9), varying the horizontal extensional velocity and the Moho temperature, which we use here as a proxy for the thermal and rheological lithospheric layering. Figures 2a–2c show the resulting strain rate at a depth of 10 km for the experiments with a boundary extensional velocity of 3 mm/yr (models 4–6). Along-axis variations in rift width develop in all experiments, with consistent narrowing over the plume. Increasing the boundary velocity results in a more distributed extension, with rift width increasing from 75–175 km to 150–425 km (widths of deformation zones are measured in the center of the model domain along the blue lines shown on Figures 2a–2c) when the boundary velocity increases from 1.5 to 6 mm/yr (Figure 2d). Increasing the lithospheric geotherm has the opposite effect of narrowing the rift: An increase in Moho temperature from 600 to 800°C reduces rift width from 175–425 km to 75–150 km (Figure 2d). Note that the areas away from the plume also show this narrowing under higher geothermal gradients (Figures 2a–2c).

This result contradicts the usual inference, derived from passive rifting models, that a warm (weak) lithospheric mantle produces wide rift zones, whereas a cold (high-strength) sub-Moho mantle is promptly

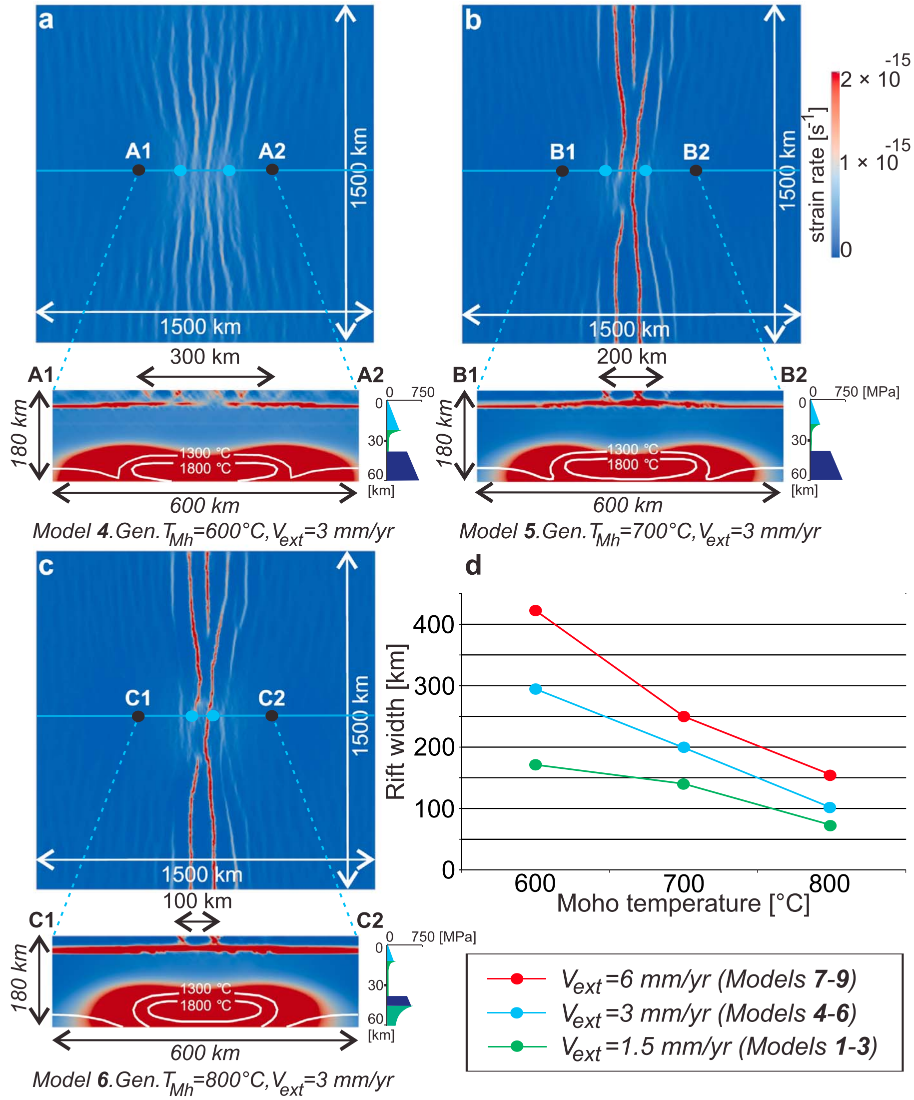

Figure 2. (a–c) Strain rate shown on horizontal (at model depth of 10 km) and vertical sections for the experiments with boundary extensional velocity of 3 mm/yr (models 4–6) and Moho temperature (T_{Mh}) of (a) 600°C, (b) 700°C, and (c) 800°C after 3 Myr. The blue circles indicate the boundary of the deformation zone across the center of the model domain (i.e., along the blue line). The white lines on the cross section show the 1,300 and 1,800°C isotherms, corresponding to the lithosphere-asthenosphere boundary, and the outline of the plume head (see also inset in Figure 3b), respectively. The initial rheological structure is shown for each experiment by a schematic vertical profile. (d) Width of the rift zone as a function of Moho temperature for boundary extensional velocities (V_{ext}) of 1.5 mm/yr (models 1–3), 3 mm/yr (models 4–6), and 6 mm/yr (models 7–9) shown by green, blue, and red lines, respectively. Note that a characteristic hour glass rifting pattern develops in all experiments (see plan views) because of increased decoupling within the lithosphere in the central part of the model due to the thermal effect of the plume material. In the lower part of the vertical sections, the bulk of high strain rates refers to deformation associated with hot plume material ponding at the base of the lithosphere. A higher geotherm favors a deeper penetration of the plume into the lowermost lithospheric mantle. In contrast, a colder geotherm results in wider lateral spreading with a concave shape of plume head-related deformation zone.

subjected to localized strain in areas of preimposed lithospheric weakness (Brun, 1999; Buck, 1991; Gueydan et al., 2008). In passive rifting experiments, fast strain localization in the brittle lithospheric mantle usually develops from the combination of large far-field forcing and a preimposed weak seed localized in space at the start of rifting. On the contrary, our active-passive models are consistent with ultraslow extension rates and a broad, warmer than average upper mantle plume, two key features observed in the central EARS (Birhanu et al., 2016; Calais et al., 1998; Nyblade et al., 2000; O'Donnell et al., 2013; Saria et al., 2014). We find that these conditions are not sufficient for large faults to propagate through the high-strength

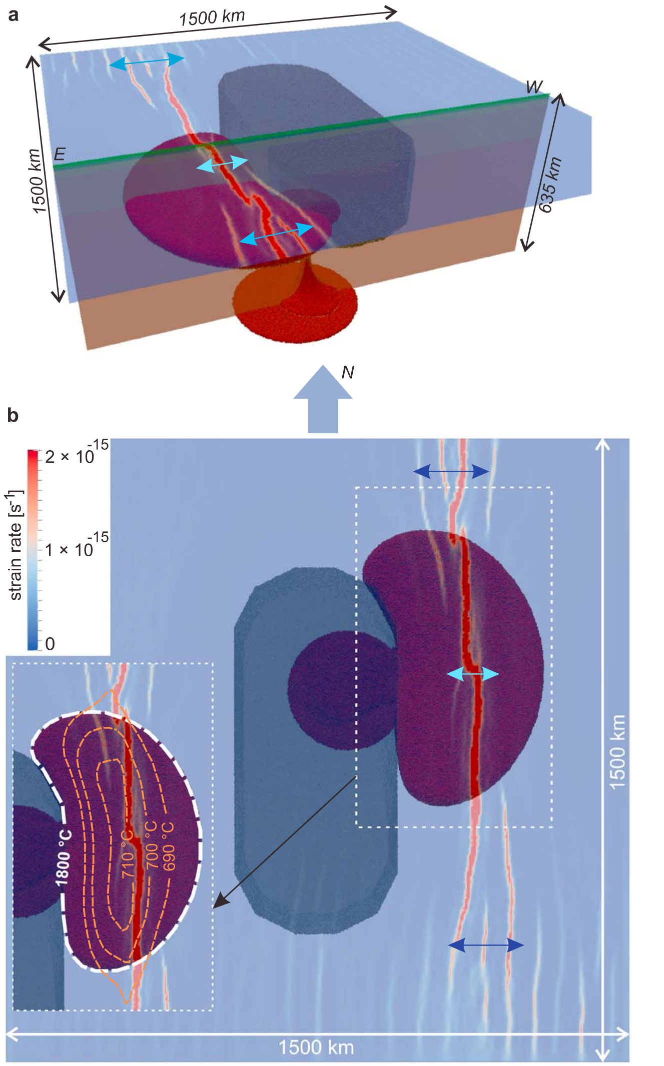

Figure 3. Numerical experiment with a craton embedded into the lithosphere and a mantle plume initially shifted to the northeast with respect to the craton center (model 10. EARS.T_{Mh} = 700°C, V_{ext} = 3 mm/yr; see Table 2) after 4 Myr. (a) 3-D view of the main model features. The plume material is shown in dark red; the craton is the dark blue volume. (b) Top view of the along-axis transition between narrow and wide rifts. The dark blue arrows indicate the zones of wide deformation, whereas the light blue one illustrates the narrow rift segment above hot mantle plume material ponding at the bottom of the lithosphere to the northeast of the craton. Left bottom inset: The white line refers to the 1,800°C isotherm at the lithosphere-asthenosphere boundary (150 km); the orange lines (790–810°C isotherms) illustrate the plume-induced thermal perturbation at 35.5 km depth (i.e., 500 m above the Moho).

uppermost lithospheric mantle but lead to a long stage of extensional deformation in an upper crust rheologically decoupled from the sub-Moho mantle by a ductile lower crust. In the models, brittle deformation in the upper crust localizes as a result of the compensating ductile flow of lower-crustal material (see cross sections in Figure 2). The width of this deforming zone is therefore controlled by the degree of rheological coupling between the brittle upper crust and the lithospheric mantle (the more decoupled the system, the narrower the deformation) that, in turn, is determined by the initial lithospheric geotherm.

During their long, initial evolution stage, our models share similarities with the “core-complex” extension mode of Buck (1991), which develops under conditions of high Moho temperature and low strain rate. In both cases deformation is accommodated by faulting in the upper crust and diffuse flow in the ductile lower crust, thus keeping the Moho flat and the lithospheric mantle almost undeformed. In contrast with Buck (1991), our models remain in the ultraslow extension regime (a few mm/yr over a few hundred kilometers), as observed in the EARS, and therefore do not reproduce the classical “lithospheric-scale” rifting with localized strain along normal faults that cut through the entire lithosphere, with significant lateral gradients in crustal and lithospheric thicknesses.

A slightly more complex model setup, with a craton embedded in the EARS lithosphere (model 10), is shown on Figure 3. Similarly to previous 3-D experiments (Burov & Gerya, 2014; Koptev et al., 2015, 2016, 2018), this model predicts a rapid mantle ascent (vertical speed of ~80 cm/yr) with the plume head reaching the base of the lithosphere 0.5 Myr into the model evolution. The plume material is then deflected to the eastern side of the craton, where it generates a broad topographic high reaching a maximum of 2 km similar in spatial extent to the Kenya dome of the central EARS (Figure 1). After 1 to 2 Myr, extensional deformation localizes through the topographic dome and splits it in two along a narrow rift basin with maximum strain localization at the apex of the dome, coincident with the maximum thermal effect of the plume material, that is, the maximal decoupling within the lithosphere. The thermal influence of the plume head and its buoyancy-driven mechanical effect decrease to the north and south, resulting in extensional deformation distributed across an area that is at least twice as broad, with the formation of several subparallel rift basins (Figure 3b). This setting is similar to the transition observed between the narrow Kenya rift and the broader Turkana depression to the north and the multibasin Tanzania divergence to the south (Figure 1).

The sensitivity of the models results to parameters such as the size, temperature, and density of the mantle plume or extension rate has been thoroughly investigated in previous work, although for broader-scale setups (Koptev et al., 2015, 2016). Varying mantle plume parameters and the far-field extension rate only affects the timing of plume impingement at the base of the lithosphere and the absolute values of localized strain rates, respectively, while rifting style and geometry remain the same. Small variations in the craton configuration do not affect the model features, which are mostly controlled by the plume head impingement on the base of the lithosphere to the east of the craton. Total strain over the course of the model evolution, localized on one or several basins (depending on rift width), amounts to 12 to 37 km of total extension, in accord with geological estimates of 10 to 40 km from the Kenyan rift to Turkana (Hendrie et al., 1994; KRISP Working Group, 1991; Morley et al., 1992, 1999). This agreement is, however, not an accurate model validation as geological estimates remain largely uncertain and model parameters were not specifically tuned to match the details of the EARS geology.

4. Discussion and Conclusion

Model results predicting along-strike rift width variations are consistent with the observation of a narrow Kenya rift coincident with the maximum uplift—and warmer—region of the eastern branch of the EARS, while the rift broadens to the north and south as the influence of the plume decreases. This result, counter-intuitive in the framework of passive rifting models that assume large far-field forcing together with predefined weak zones, finds a simple explanation in the active-passive framework advocated for here. Model simulations indicate that rift width variations develop as a consequence of spatial variations of the lithospheric geotherm associated with the evolving mantle plume impinging underneath a prestressed lithosphere under very slow extension. In this framework, narrow rifts occur spontaneously, without the need for an ad hoc weak zone between the craton and the embedding lithosphere since the plume acts to weaken the lithosphere and focus brittle strain in the crust (Burov & Gerya, 2014).

Along-axis variations of rift width similar to the eastern branch of the EARS are also observed in the Baikal rift system, whose narrow southwestern basin at the Siberian craton border widens to the northeast, transitioning to diffuse deformation in the Sayan-Baikal belt (Petit & Déverchère, 2006). Similarly to the Kenya rift, the narrow southwestern segment of the Baikal rift is associated with an upwarped lithosphere/asthenosphere interface (Gao et al., 2003) interpreted either as an ascending branch of small-scale convection (e.g., Huismans et al., 2001) or as a narrow mantle plume that reaches the bottom of the cold Siberian craton and follows its border in the Baikal area (e.g., Petit & Déverchère, 2006).

It is commonly assumed that normal faults localize within mobile belts along the edges of cratonic blocks (e.g., Corti et al., 2007; Guillou-Frottier et al., 2012; Ring, 1994; Tommasi & Vauchez, 2001). Our experiments, supported by observations in the East African and Baikal rift systems, show that the localization and style of continental rifting in a coupled mantle-lithosphere system are controlled by the presence and location of warm mantle material ponding at the lithosphere-asthenosphere boundary and channeled under areas of lithospheric thinning. Regardless of preexisting lithospheric heterogeneities, such coupled mantle-lithosphere system can evolve into complex rift zones whose width and magmatic characteristics vary significantly along-axis.

Acknowledgments
We thank Luke Mondy and an anonymous reviewer for their constructive comments that contributed to improving the manuscript. This study is cofunded by the Advanced ERC Grant 290864 RHEOLITH (E. Burov-A. Koptev) and ERC Consolidator Grant 615703 EXTREME (T. Ehlers-A. Koptev), as well as a U.S. National Science Foundation grant EAR-0538119 and French INSU-CNRS program Tellus-Rift (E. Calais). The numerical simulations were performed on the ERC-funded SGI Ulysse cluster of ISTEP. The computer code I3ELVIS used to generate our 3-D thermomechanical numerical model is provided in Gerya (2010). Open source software ParaView (http://www.paraview.org) was used for 3-D visualization. Modeling results in ParaView format are available at https://drive.google.com/open?id=1PqnLmtYWuEJ41U4RGACAtlncqdPURQj7.

References

Adams, A., Nyblade, A., & Weeraratne, D. (2012). Upper mantle shear wave velocity structure beneath the East African plateau: Evidence for a deep, plateauwide low velocity anomaly. *Geophysical Journal International*, *189*(1), 123–142. https://doi.org/10.1111/j.1365-246X.2012.05373.x

Albaric, J., Déverchère, J., Petit, C., Perrot, J., & Le Gall, B. (2009). Crustal rheology and depth distribution of earthquakes: Insights from the central and southern East African Rift System. *Tectonophysics*, *468*(1-4), 28–41. https://doi.org/10.1016/j.tecto.2008.05.021

Artemieva, I. M. (2006). Global 1×1 thermal model TC1 for the continental lithosphere: Implications for lithosphere secular evolution. *Tectonophysics*, *416*(1-4), 245–277. https://doi.org/10.1016/j.tecto.2005.11.022

Beniest, A., Koptev, A., & Burov, E. (2017). Numerical models for continental break-up: Implications for the South Atlantic. *Earth and Planetary Science Letters*, *461*, 176–189. https://doi.org/10.1016/j.epsl. 2016.12.034

Beniest, A., Koptev, A., Leroy, S., Sassi, W., & Guichet, X. (2017). Two-branch break-up systems by a single mantle plume: Insights from numerical modeling. *Geophysical Research Letters*, *44*, 9589–9597. https://doi.org/10.1002/2017GL074866

Birhanu, Y., Bendick, R., Fisseha, S., Lewi, E., Floyd, M., King, R., & Reilinger, R. (2016). GPS constraints on broad scale extension in the Ethiopian Highlands and Main Ethiopian Rift. *Geophysical Research Letters*, *43*, 6844–6851. https://doi.org/10.1002/2016GL069890

Braile, L. W., Keller, G. R., Wendlandt, R. F., Morgan, P., & Khan, M. A. (2006). The East African Rift System. *Developments in Geotectonics*, *25*, 213. https://doi.org/10.1016/S0419-0254(06)80013-3

Brun, J. P. (1999). Narrow rifts versus wide rifts: Inferences for mechanics of rifting from laboratory experiments. *Philosophical Transactions of the Royal Society of London*, *357*, 695–712. https://doi.org/10.1098/rsta.1999.0349

Brune, S., Corti, G., & Ranalli, G. (2017). Controls of inherited lithospheric heterogeneity on rift linkage: Numerical and analog models of interaction between the Kenyan and Ethiopian rifts across the Turkana depression. *Tectonics*, *36*, 1767–1786. https://doi.org/10.1002/2017TC004739

Buck, W. R. (1991). Models of continental lithospheric extension. *Journal of Geophysical Research*, *96*, 20,161–20,178. https://doi.org/10.1029/91JB01485

Buck, W. R. (2006). The role of magma in the development of the Afro-Arabian Rift System. *Geological Society of London, Special Publications*, *259*(1), 43–54. https://doi.org/10.1144/GSL.SP.2006.259.01.05

Burov, E. (2011). Rheology and strength of the lithosphere. *Marine and Petroleum Geology*, *28*(8), 1402–1443. https://doi.org/10.1016/j.marpetgeo.2011.05.008

Burov, E., & Cloetingh, S. (2010). Plume-like upper mantle instabilities drive subduction initiation. *Geophysical Research Letters*, *37*, L03309. https://doi.org/10.1029/2009GL041535

Burov, E., & Gerya, T. (2014). Asymmetric three-dimensional topography over mantle plumes. *Nature*, *513*(7516), 85–89. https://doi.org/10.1038/nature13703

Burov, E., & Guillou-Frottier, L. (2005). The plume head-continental lithosphere interaction using a tectonically realistic formulation for the lithosphere. *Geophysical Journal International*, *161*(2), 469–490. https://doi.org/10.1111/j.1365-246X.2005.02588.x

Calais, E., Lesne, O., Déverchère, J., San'kov, V., Lukhnev, A., Miroshnitchenko, A., et al. (1998). Crustal deformation in the Baikal rift from GPS measurements. *Geophysical Research Letters*, *25*, 4003–4006. https://doi.org/10.1029/1998GL900067

Chang, S. J., Ferreira, A. M. G., Ritsema, J., Heijst, H. J., & Woodhouse, J. H. (2015). Joint inversion for global isotropic and radially anisotropic mantle structure including crustal thickness perturbations. *Journal of Geophysical Research: Solid Earth*, *120*, 4278–4300. https://doi.org/10.1002/2014JB011824

Chang, S. J., & Van der Lee, S. (2011). Mantle plumes and associated flow beneath Arabia and East Africa. *Earth and Planetary Science Letters*, *302*(3-4), 448–454. https://doi.org/10.1016/j.epsl.2010.12.050

Corti, G., Iandelli, I., & Cerca, M. (2013). Experimental modeling of rifting at craton margins. *Geosphere*, *9*(1), 138–154. https://doi.org/10.1130/GES00863.1

Corti, G., van Wijk, J., Cloetinhg, S., & Morley, C. K. (2007). Tectonic inheritance and continental rift architecture: Numerical and analogue models of the East African Rift System. *Tectonics*, *26*, TC6006. https://doi.org/10.1029/2006TC002086

Dawson, J. (1992). Neogene tectonics and volcanicity in the North Tanzania Sector of the Gregory Rift Valley: Contrasts with the Kenya sector. *Tectonophysics*, *204*(1-2), 81–92. https://doi.org/10.1016/0040-1951(92)90271-7

DeMets, C., & Merkouriev, S. (2016). High-resolution estimates of Nubia-Somalia plate motion since 20 Ma from reconstructions of the Southwest Indian Ridge, Red Sea and Gulf of Aden. *Geophysical Journal International*, *207*(1), 317–332. https://doi.org/10.1093/gji/ggw276

Ebinger, C. J., Yemane, T., Harding, D. J., Tesfaye, S., Kelley, S., & Rex, D. C. (2000). Rift deflection, migration, and propagation: Linkage of the Ethiopian and Eastern rifts, Africa. *Geological Society of America Bulletin*, *112*(2), 163–176. https://doi.org/10.1130/0016-7606(2000)112%3C163:RDMAPL%3E2.0.CO;2

Fishwick, S., & Bastow, I. D. (2011). Towards a better understanding of African topography: A review of passive-source seismic studies of the African crust and upper mantle. *Geological Society of London, Special Publications*, *357*(1), 343–371. https://doi.org/10.1144/SP357.19

François, T., Koptev, A., Cloetingh, S., Burov, E., & Gerya, T. (2017). Plume-lithosphere interactions in rifted margin tectonic settings: Inferences from thermo-mechanical modelling. *Tectonophysics*. https://doi.org/10.1016/j.tecto.2017.11.027

Furman, T., Kaleta, K. M., Bryce, J. G., & Hanan, B. B. (2006). Tertiary mafic lavas of Turkana, Kenya: Constraints on East African plume structure and the occurrence of high-mu volcanism in Africa. *Journal of Petrology*, *47*(6), 1221–1244. https://doi.org/10.1093/petrology/egl009

Gao, S. S., Liu, K. H., Davis, P. M., Slack, P. D., Zorin, Y. A., Mordvinova, V. V., & Kozhevnikov, V. M. (2003). Evidence for small-scale mantle convection in the upper mantle beneath the Baikal rift zone. *Journal of Geophysical Research*, *108*(B4), 2194. https://doi.org/10.1029/2002JB002039

George, R., Rogers, N., & Kelley, S. (1998). Earliest magmatism in Ethiopia: Evidence for two mantle plumes in one flood basalt province. *Geology*, *26*(10), 923–926. https://doi.org/10.1130/0091-7613(1998)026%3C0923:EMIEEF%3E2.3.CO;2

Gerya, T. V. (2010). *Introduction to numerical geodynamic modelling* (345 pp.). Cambridge, UK: Cambridge University Press.

Gerya, T. V., & Yuen, D. A. (2007). Robust characteristics method for modelling multiphase visco-elasto-plastic thermo-mechanical problems. *Physics of the Earth and Planetary Interiors*, *163*(1-4), 83–105. https://doi.org/10.1016/j.pepi.2007.04.015

Gueydan, F., Morency, C., & Brun, J. P. (2008). Continental rifting as a function of lithosphere mantle strength. *Tectonophysics*, *460*(1-4), 83–93. https://doi.org/10.1016/j.tecto.2008.08.012

Guillou-Frottier, L., Burov, E., Cloetingh, S., Le Goff, I., Deschamps, Y., Huet, B., & Bouchot, V. (2012). Plume-induced dynamic instabilities near cratonic blocks: Implications for P-T-t paths and metallogeny. *Global and Planetary Change*, *90*, 37–50. https://doi.org/10.1016/j.gloplacha.2011.10.007

Halldórsson, S. A., Hilton, D. R., Scarsi, P., Abebe, T., & Hopp, J. (2014). A common mantle plume source beneath the entire East African Rift System revealed by coupled helium-neon systematics. *Geophysical Research Letters*, *41*, 2304–2311. https://doi.org/10.1002/2014GL059424

Hendrie, D. B., Kusznir, N. J., Morley, C. K., & Ebinger, C. J. (1994). Cenozoic extension in northern Kenya: A quantitative model of rift basin development in the Turkana region. *Tectonophysics*, *236*(1–4), 409–438. https://doi.org/10.1016/0040-1951/(94)90187-2

Huerta, A. D., Nyblade, A. A., & Reusch, A. M. (2009). Mantle transition zone structure beneath Kenya and Tanzania: More evidence for a deep-seated thermal upwelling in the mantle. *Geophysical Journal International*, *177*(3), 1249–1255. https://doi.org/10.1111/j.1365-246X.2009.04092.x

Huismans, R. S., Podladchikov, Y. Y., & Cloetingh, S. (2001). Transition from passive to active rifting: Relative importance of asthenospheric doming and passive extension of the lithosphere. *Journal of Geophysical Research*, *106*, 11,271–11,291. https://doi.org/10.1029/2000JB900424

Isola, I., Mazzarini, F., Bonini, M., & Corti, G. (2014). Spatial variability of volcanic features in early-stage rift settings: The case of the Tanzania divergence, East African Rift System. *Terra Nova*, *26*(6), 461–468. https://doi.org/10.1111/ter.12121

Katumwehe, A. B., Abdelsalam, M. G., & Atekwana, E. A. (2015). The role of pre-existing Precambrian structures in rift evolution: The Albertine and Rhino grabens, Uganda. *Tectonophysics*, *646*, 117–129. https://doi.org/10.1016/j.tecto.2015.01.022

Kendall, J. M., Pilidou, S., Keir, D., Bastow, I. D., Stuart, G. W., & Ayele, A. (2006). Mantle upwellings, melt migration and the rifting of Africa: Insights from seismic anisotropy. *Geological Society of London, Special Publications*, *259*(1), 55–72. https://doi.org/10.1144/GSL.SP.2006.259.01.06

Koptev, A., Burov, E., Calais, E., Leroy, S., Gerya, T., Guillou-Frottier, L., & Cloetingh, S. (2016). Contrasted continental rifting via plume-craton interaction: Applications to Central East African rift. *Geoscience Frontiers*, *7*(2), 221–236. https://doi.org/10.1016/j.gsf.2015.11.002

Koptev, A., Burov, E., Gerya, T., Le Pourhiet, L., Leroy, S., Calais, E., & Jolivet, L. (2017). Plume-induced continental rifting and break-up in ultra-slow extension context: Insights from 3D numerical modeling. *Tectonophysics*. https://doi.org/10.1016/j.tecto.2017.03.025

Koptev, A., Calais, E., Burov, E., Leroy, S., & Gerya, T. (2015). Dual continental rift systems generated by plume-lithosphere interaction. *Nature Geoscience*, *8*(5), 388–392. https://doi.org/10.1038/ngeo2401

Koptev, A., Cloetingh, S., Burov, E., François, T., & Gerya, T. (2017). Long-distance impact of Iceland plume on Norway's rifted margin. *Scientific Reports*, *7*(1), 10408. https://doi.org/10.1038/s41598-017-07523-y

Koptev, A., Cloetingh, S., Gerya, T., Calais, E., & Leroy, S. (2018). Non-uniform splitting of a single mantle plume by double cratonic roots: Insight into the origin of the central and southern East African Rift System. *Terra Nova*, *30*(2), 125–134. https://doi.org/10.1111/ter.12317

KRISP Working Group (1991). The Kenya Rift: Pure shear extension above a mantle plume. *Nature*, *345*, 223–227.

Laó-Dávila, D. A., Al-Salmi, H. S., Abdelsalam, M. G., & Atekwana, E. A. (2015). Hierarchical segmentation of the Malawi Rift: The influence of inherited lithospheric heterogeneity and kinematics in the evolution of continental rifts. *Tectonics*, *34*, 2399–2417. https://doi.org/10.1002/2015TC003953

Le Gall, B., Gernigon, L., Rolet, J., Ebinger, C., Gloaguen, R., Nilsen, O., et al. (2004). Neogene-Holocene rift propagation in Central Tanzania: Morphostructural and aeromagnetic evidence from the Kilombero area. *Geological Society of America Bulletin*, *116*(3), 490–510. https://doi.org/10.1130/B25202.1

Le Gall, B., Nonnotte, P., Rolet, J., Benoit, M., Guillou, H., Mousseau-Nonnotte, M., et al. (2008). Rift propagation at craton margin. Distribution of faulting and volcanism in the North Tanzanian Divergence (East Africa) during Neogene times. *Tectonophysics*, *448*(1–4), 1–19. https://doi.org/10.1016/j.tecto.2007.11.005

Lithgow-Bertelloni, C., & Silver, P. G. (1998). Dynamic topography, plate driving forces and the African superswell. *Nature*, *395*(6699), 269–272. https://doi.org/10.1038/26212

MacDonald, R., Rogers, N. W., Fitton, J. G., Black, S., & Smith, M. (2001). Plume-lithosphere interactions in the generation of the basalts of the Kenya Rift, East Africa. *Journal of Petrology*, *42*(5), 877–900. https://doi.org/10.1093/petrology/42.5.877

Melnick, D., Garcin, Y., Quinteros, J., Strecker, M. R., Olago, D., & Tiercelin, J. J. (2012). Steady rifting in northern Kenya inferred from deformed Holocene lake shorelines of the Suguta and Turkana basins. *Earth and Planetary Science Letters*, *331*, 335–346. https://doi.org/10.1016/j.epsl.2012.03.007

Morley, C., Karanja, F., Wescott, W., Stone, D., Harper, R., Wigger, S., & Day, R. (1999). Geology and geophysics of the western Turkana basins, Kenya. In C. K. Morley (Ed.), *Geoscience of Rift Systems – Evolution of East Africa: AAPG Studies in Geology* (Vol. 44, pp. 15–54). Tulsa: American Association of Petroleum Geologists.

Morley, C. K. (2010). Stress re-orientation along zones of weak fabrics in rifts: An explanation for pure extension in 'oblique' rift segments? *Earth and Planetary Science Letters*, *297*(3-4), 667–673. https://doi.org/10.1016/j.epsl.2010.07.022

Morley, C. K., Wescott, W. A., Stone, D. M., Harper, R. M., Wigger, S. T., & Karanja, F. M. (1992). Tectonic evolution of the northern Kenyan Rift. *Journal of the Geological Society*, *149*(3), 333–348. https://doi.org/10.1144/gsjgs.149.3.0333

Mulibo, G. D., & Nyblade, A. A. (2013). Mantle transition zone thinning beneath eastern Africa: Evidence for a whole-mantle superplume structure. *Geophysical Research Letters*, *40*, 3562–3566. https://doi.org/10.1002/grl.50694

Nyblade, A. A. (1997). Heat flow across the east African Plateau. *Geophysical Research Letters*, *24*, 2083–2086. https://doi.org/10.1029/97GL01952

Nyblade, A. A., Owens, T. J., Gurrola, H., Ritsema, J., & Langston, C. A. (2000). Seismic evidence for a deep upper mantle thermal anomaly beneath east Africa. *Geology*, *28*(7), 599–602. https://doi.org/10.1130/0091-7613(2000)28%3C599:SEFADU%3E2.0.CO;2

O'Connor, J. M., Stoffers, P., van den Bogaard, P., & McWilliams, M. (1999). First seamount age evidence for significantly slower African plate motion since 19 to 30 Ma. *Earth and Planetary Science Letters*, *171*(4), 575–589. https://doi.org/10.1016/S0012-821X(99)00183-1

O'Donnell, J. P., Adams, A., Nyblade, A. A., Mulibo, G. D., & Tugume, F. (2013). The uppermost mantle shear wave velocity structure of eastern Africa from Rayleigh wave tomography: Constraints on rift evolution. *Geophysical Journal International*, *194*(2), 961–978. https://doi.org/10.1093/gji/ggt135

Pérez-Gussinyé, M., Metois, M., Fernández, M., Vergés, J., Fullea, J., & Lowry, A. R. (2009). Effective elastic thickness of Africa and its relationship to other proxies for lithospheric structure and surface tectonics. *Earth and Planetary Science Letters*, *287*(1-2), 152–167. https://doi.org/10.1016/j.epsl.2009.08.004

Petit, C., & Déverchère, J. (2006). Structure and evolution of the Baikal rift: A synthesis. *Geochemistry, Geophysics, Geosystems*, *7*, Q11016. https://doi.org/10.1029/2006GC001265

Pik, R., Marty, B., & Hilton, D. R. (2006). How many mantle plumes in Africa? The geochemical point of view. *Chemical Geology*, *226*(3-4), 100–114. https://doi.org/10.1016/j.chemgeo.2005.09.016

Ring, U. (1994). The influence of preexisting structure on the evolution of the Cenozoic Malawi Rift (East African Rift System). *Tectonics*, *13*, 313–326. https://doi.org/10.1029/93TC03188

Ring, U. (2014). The East African Rift System. *Austrian Journal of Earth Sciences*, *107*(1), 132–146.

Ring, U., Betzler, C., & Delvaux, D. (1992). Normal vs. strike-slip faulting during rift development in East Africa: The Malawi rift. *Geology*, *20*(11), 1015–1018. https://doi.org/10.1130/0091-7613%20(1992)020%3C1015:NVSSFD%3E2.3.CO;2

Ritsema, J., Nyblade, A. A., Owens, T. J., & Langston, C. A. (1998). Upper mantle seismic velocity structure beneath Tanzania, East Africa: Implications for the stability of cratonic lithosphere. *Journal of Geophysical Research*, *103*, 21,201–21,213. https://doi.org/10.1029/98JB01274

Ritsema, J., van Heijst, H. J., & Woodhouse, J. H. (1999). Complex shear wave velocity structure imaged beneath Africa and Iceland. *Science*, *286*(5446), 1925–1928. https://doi.org/10.1126/science.286.5446.1925

Rooney, T. O. (2017). The Cenozoic magmatism of East Africa: Part I—Flood basalts and pulsed magmatism. *Lithos*, *286–287*, 264–301. https://doi.org/10.1016/j.lithos.2017.05.014

Saria, E., Calais, E., Stamps, D. S., Delvaux, D., & Hartnady, C. J. H. (2014). Present-day kinematics of the East African Rift. *Journal of Geophysical Research*, *119*, 3584–3600. https://doi.org/10.1002/2013JB010901

Tommasi, A., & Vauchez, A. (2001). Continental rifting parallel to ancient collisional belts: An effect of the mechanical anisotropy of the lithospheric mantle. *Earth and Planetary Science Letters*, *185*(1-2), 199–210. https://doi.org/10.1016/S0012-821X(00)00350-2

Van der Hilst, R. D., Widiyantoro, S., & Engdahl, E. R. (1997). Evidence for deep mantle circulation from global tomography. *Nature*, *386*(6625), 578–584. https://doi.org/10.1038/386578a0

Versfelt, J., & Rosendahl, B. R. (1989). Relationships between pre-rift structure and rift architecture in Lakes Tanganyika and Malawi, East Africa. *Nature*, *337*(6205), 354–357. https://doi.org/10.1038/337354a0

Vetel, W., Le Gall, B., & Johnson, T. C. (2004). Recent tectonics in the Turkana Rift (North Kenya): An integrated approach from drainage network, satellite imagery and reflection seismic analyses. *Basin Research*, *16*(2), 165–181. https://doi.org/10.1046/j.1365-2117.2003.00227.x

Zeyen, H., Volker, F., Wehrle, V., Fuchs, K., Sobolev, S. V., & Altherr, R. (1997). Styles of continental rifting: Crust-mantle detachment and mantle plumes. *Tectonophysics*, *278*(1–4), 329–352. https://doi.org/10.1016/S0040-1951(97)00111-X